

Compact Lyman- α Emitting Candidates at $z \simeq 2.4$ in Deep Medium-band *HST*¹ *WFPC2* Images

Sebastian M. Pascarelle

Dept. of Physics & Astronomy, SUNY Stony Brook, Stony Brook, NY 11794

Rogier A. Windhorst

Dept. of Physics & Astronomy, Arizona State University, Tempe, AZ 85287

and

William C. Keel

Dept. of Physics & Astronomy, University of Alabama, Tuscaloosa, AL 35487

ABSTRACT

Medium-band imaging with HST/WFPC2 in the F410M filter has previously revealed a population of compact Lyman- α emission objects around the radio galaxy 53W002 at $z \simeq 2.4$. We report detections of similar objects at $z \simeq 2.4$ in random, high-latitude HST parallel observations of three additional fields, lending support to the idea that they constitute a widespread population at these redshifts. The three new fields contain 18 Lyman- α candidates, in contrast to the 17 detected in the deeper exposure of the single WFPC2 field around 53W002. We find substantial differences in the number of candidates from field to field, suggesting that significant large-scale structure is already present in the galaxy distribution at this cosmic epoch. The likely existence of $z \simeq 2.4$ sub-galactic clumps in several random fields shows that these objects may have been common in the early universe and strengthens the argument that such objects may be responsible for the formation of a fraction of the luminous present-day galaxies through hierarchical merging.

Subject headings: galaxies: evolution—galaxies: formation—cosmology: large-scale structure of universe

¹Based on observations with the NASA/ESA *Hubble Space Telescope* obtained at the Space Telescope Science Institute, which is operated by AURA, Inc., under NASA Contract NAS 5-26555.

1. Introduction

The formation of structure in the universe, from the largest scales (*e.g.*, “great walls”) to the smallest scales (*e.g.*, galaxies and globular clusters), remains a very controversial topic in modern observational cosmology. Standard inflationary cosmologies predict that the primordial density field is a Gaussian random field which can lead to either “top-down” or “bottom-up” structure formation, depending on whether very small or very large structures formed first. This in turn depends upon whether the gravitationally dominant dark matter is cold (CDM), hot (HDM), or some mixture thereof (CHDM, MDM).

Traditionally, it has been assumed that a dominant dissipationless component of dark matter accumulates through gravitational instability into clumps, the virialized parts of which become dark matter halos. Galaxies then form by the cooling and condensation of gas within these halos (White & Rees 1978). The inability to detect the intense Lyman- α emission expected from large numbers of such young forming galaxies with strong continuous star formation at high redshift in narrow-band imaging surveys (Thompson, Mannucci, & Beckwith 1996; Thompson, Djorgovski, & Trauger 1995) is instead more consistent with a hierarchical formation scenario, in which galaxies were assembled from pieces over a long interval. It is also possible that high-redshift galaxies, or more specifically, their Lyman- α light is obscured by dust or destroyed by resonant scattering, even in the absence of dust. Still, hierarchical clustering (a “bottom-up” scenario) currently appears to be the most successful at reproducing many of the properties of the real universe, as noted by Diaferio & Geller (1997), while remaining within the constraints produced by the COBE results. In the typical (CDM) hierarchical clustering model, structure grows from the gravitational collapse of small initial density perturbations, from which systems of progressively larger mass merge and collapse to form newly virialized systems. Most modern hierarchical models are variations of the original Press-Schechter (1974) theory of structure formation, in which isothermal “seeds” existing at recombination grew into the galaxies we see today.

Pascarelle *et al.* (1996b, hereafter P96b) presented evidence for a gravitationally bound collection of sub-galactic star-forming objects at $z \simeq 2.4$, which fits well with expectations from hierarchical galaxy formation. These objects appear to have effective radii (or half-light radii) of $r_e \lesssim 0''.1$, or $\lesssim 1$ kpc (assuming $H_0 = 100 \text{ km s}^{-1} \text{ Mpc}^{-1}$, $q_0 = 0.5$ throughout, unless otherwise noted). Since this is much smaller than the median *WFPC2* field galaxy scale length of $\simeq 0''.3$ (Odewahn *et al.* 1996), and at any redshift in the range $z \simeq 0.3 - 3$, $0''.1 - 0''.2$ corresponds to only 0.5–2 kpc, the $z \simeq 2.4$ candidates appear to be smaller than the size of a present-day galaxy (*i.e.*, sub-galactic). P96b suggested that these proposed “galaxy building blocks” are actually part of a widespread population existing throughout the redshift range $z \simeq 2 - 5$. We undertook a Cycle 6 *HST* project to image four random fields using the same

filters as P96b (since WFPC2 conveniently has a medium-band filter to sample Lyman- α at $z \simeq 2.4$) in an effort to test the universality of these objects at $z \simeq 2.4$.

It is clear that galaxies at all redshifts are more inclined to be in groups or clusters than isolated, giving the term “field galaxy” less meaning than it once had. As such, it is perhaps not surprising to find that in many “pencil-beam” galaxy redshift surveys, often several galaxies are found in a single narrow redshift bin (*e.g.*, the Hubble Deep Field (HDF) counts reported in Cohen *et al.* 1996 and the large structure of galaxies found at $z \simeq 3$ by Steidel *et al.* 1998). On a slightly larger angular scale, “spikes” have been found in the redshift distribution of several more extensive galaxy surveys out to $z \lesssim 1$ (Broadhurst *et al.* 1990; Landy *et al.* 1996; Ettori, Guzzo & Tarenghi 1997), indicative of some sort of larger structure at earlier epochs. What is questionable, according to CDM models, is whether or not any such structure could have existed at high redshifts. Rauch, Haehnelt, & Steinmetz (1997, hereafter RHS97) are able to reproduce the observational characteristics of QSO absorption systems at $z \sim 3$ over a wide range of column densities with a model consisting of sub-galactic clumps embedded in sheet-like structures and often lying along filaments. The similarities between the grouping of $z \simeq 2.4$ sub-galactic clumps of P96b (see their Fig. 1) and the RHS97 simulations are quite striking (see Fig. 1a of RHS97, which shows not only a field about the same size as our 53W002 WFPC2 field, but also with about the same number of clumps at a similarly high redshift). Their simulations indicate that ~ 20 compact clumps will merge to produce about three L^* galaxies by $z=0$. This agrees quite well with the calculations carried out in P96b, which suggest that 17 candidate subgalactic clumps could form several L^* galaxies by $z=0$. Is it possible that groups, clusters, or even larger-scale structure existed to some extent at earlier epochs, although at much lower amplitude than that seen at lower redshifts? If the answer is yes, then it should not be surprising to find the compact, star-forming protogalactic objects arranged in groups, clusters, or even filaments or “sheets.” The Cycle 6 data presented here represent an initial attempt to begin to answer this question.

In §2, we describe the observations and data processing, in §3 we present the results, and in §4 we discuss some of the implications of these results in the context of galaxy and structure formation at high redshift. Our conclusions are summarized in §5.

2. Observations

HST has the ability to image a field with WFPC2 in parallel with other instruments. This (usually) random field can be $4'$ – $14'$ away from the primary target, depending on the primary instrument being used. We received three long parallel observations with WFPC2

using the F410M, F450W, and F814W filters in Cycle 6. The medium-band F410M filter is centered at 4090Å with a full-width-at-half-maximum of 150Å, so that Lyman- α emission from objects in the range $z \simeq 2.30 - 2.42$ can be detected. We received 6–8 parallel orbits per field, divided where possible into more than one exposure to allow proper cosmic ray removal (see Windhorst *et al.* 1994b). The details of the observations, including the dates, coordinates, position angle of the V3 axis, and total exposure times in each filter are given in Table 1.

Table 1: Cycle 6 Parallel Observations

date	α^a	δ	PA of V3	t_{exp} (F410M)	t_{exp} (F450W)	t_{exp} (F814W)
30 Aug 1996	21 ^h 7 ^m 31 ^s .8	−5°22′33″.1	275°0	9600s	2900s	700s
11 Jan 1997	16 ^h 36 ^m 38 ^s .3	+82°34′13″.6	127°3	11900s	3200s	900s
20 May 1997	10 ^h 24 ^m 38 ^s .1	+47°4′39″.6	290°0	14900s	5600s	3000s

^aCoordinates are J2000 and are for the *WFPC2* field center

The images were processed by the usual *HST* pipeline, and aligned to the nearest integer pixel in IRAF. For accurate photometry of compact objects that are expected to have sizes of only a few *WFPC2* pixels or less, it is imperative to do reliable cosmic ray rejection. Because of this, the averaging and cosmic ray rejection were done with a custom-written code created to deal specifically with a small number ($n \leq 4$) of low-signal images. This routine, written in the Interactive Data Language (IDL), first scales the input images by their respective exposure times. Any remaining differences left in the global sky values are from time-dependent variations in the sky background. These variations are likely due to the proximity of any particular image pointing to the earth’s limb, which changes during each orbit, so that the sky differences are additive. The program calculates rough sky values from the global image modes, and applies zeropoint offsets (by subtracting a constant) to bring all the sky values to the lowest sky in the normalized set. The image mode is calculated by fitting a polynomial to the histogram of pixel values and finding the maximum of the curve (*i.e.*, the mode). Because the cosmic ray rejection code assumes all pixels values within a few sigma of sky are “good,” it is important to remove all bad negative pixels first. Therefore, all negative pixels more than 3.5σ below the median of the eight surrounding pixels are replaced by that median.

The main loop to remove cosmic rays works by “stacking” the aligned images on top of each other and then working on each individual “stack” of pixels (or array of pixels in the z -dimension), after each pixel stack is sorted by value in ascending order. The two pixels with the lowest values are compared to see if they are $<2.5 \times \sigma$ apart, where σ is the standard

deviation using the lowest pixel value. If so, then they are averaged, and the next highest value pixel is compared to this average, and so on for the entire pixel stack. If a pixel has a value $>2.5\times\sigma$ from this running average, then it is rejected as a cosmic ray. The cutoff value of $2.5\times\sigma$ comes from Windhorst, Franklin, & Neuschaefer (1994b), who determined this as the optimal level at which to reject cosmic rays from multi-orbit *WF/PC* images. The standard deviation (σ) of the running average is recalculated at each step for each pixel stack using the CCD equation:

$$\sigma = \sqrt{Sg + RN^2 + Dt}$$

in which S = the intensity (in ADU) of that pixel, g = the CCD gain (in electrons/data number), RN = the CCD readnoise (in electrons), D = the CCD dark current (in electrons/second), and t = the exposure time (in seconds). The values for the gain, readnoise, and dark current were obtained from the *WFPC2* handbook.

Photometry was then performed, as detailed in Windhorst *et al.* (1991), on the cleaned average images using the CASSANDRA photometry package of D. Schneider, which utilizes user-input apertures and sky regions. The sky region is interpolated underneath the object aperture by fitting a sloped plane to the pixels unaffected by faint neighbors (see also Odewahn *et al.* 1996). The photometric zeropoints used are those given in Holtzman *et al.* (1995) and include the various gain ratios for each chip ($\simeq 19.55$ for F410M, $\simeq 21.92$ for F450W, and $\simeq 21.59$ for F814W). A total of 141 objects were detected simultaneously in all three filters in the three fields. The photometric “curve of growth” was examined, and apertures were adjusted to give the highest signal-to-noise ratio for each object, while maintaining the *same size* aperture in the three filters.

3. Results

3.1. New $z \simeq 2.4$ Candidates

The results of the photometry performed on the three Cycle 6 *HST* fields are presented in the color-color diagram of Figure 1 (the same as that used to identify the $z \simeq 2.4$ candidates of Pascarelle *et al.* (1996a) and P96b). For consistency with the Cycle 5 53W002 field data, we interpolated $B_{F450W} - V_{F606W}$ colors from the $B_{F450W} - I_{F814W}$ colors using the effective central wavelengths (from the *WFPC2* handbook) of the three filters involved. This approximation is justified as long as the spectra of these faint blue objects are close to a power law across the three filters (see Windhorst *et al.* 1991; P96b) and affects only the horizontal axis. As such, this approximation has almost no effect on the nearly horizontal distribution of points and the number of Lyman- α emitting candidates found.

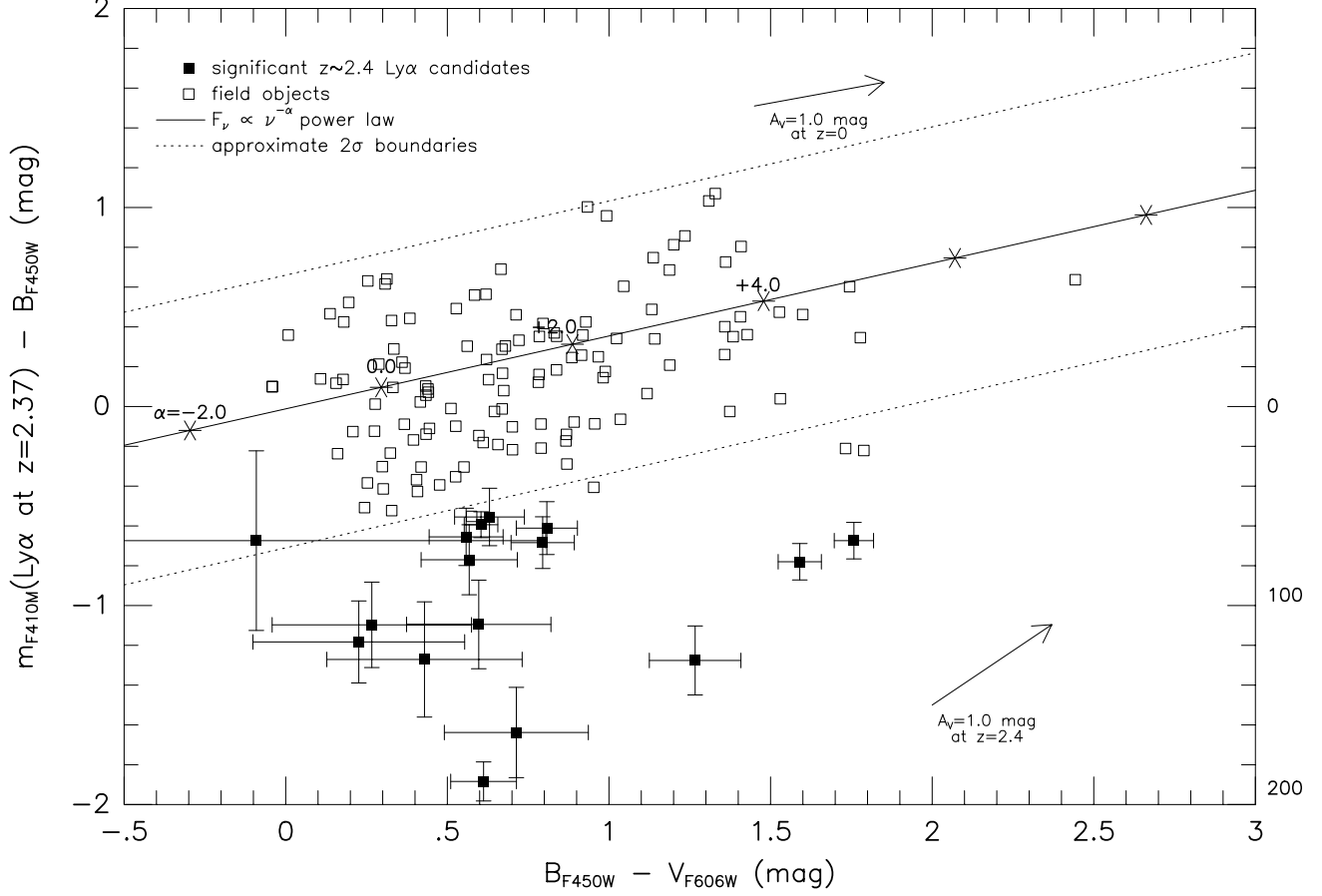


Fig. 1.— $(m_{F410M} - B_{F450W})$ versus $(B_{F450W} - V_{F606W})$ color-color diagram for 145 objects detected in the three Cycle 6 fields. The open squares are field objects and are grouped around the featureless power-law line. The dotted lines represent approximate 2σ errors in the photometry, and contain most of the field objects. Below the lower boundary is a population of objects, represented by filled squares with errorbars, which have excess emission in the F410M filter. As described in the text, most of these candidates are likely Lyman- α emitters at $z \simeq 2.4$. Unfilled squares below the lower 2σ boundary are candidates that were rejected as stars by inspection. Approximate restframe equivalent widths are indicated along the righthand axis, and show that most candidates have $W_{\text{Ly}\alpha} < 100 \text{\AA}$.

A featureless power law ($F_\nu \propto \nu^{-\alpha}$) is indicated by the solid line, with asterisks indicating integer values of α . Because of the relatively small range of the restframe spectral energy distribution (SED) that the HST filters will sample below the 4000Å break for objects at high redshift, a power law provides an adequate fit to their SEDs for various values of α . Since a large fraction of high-redshift objects are blue and have relatively uncomplicated SEDs of blue stars shortward of the 4000Å break, an α of ~ 2 would be appropriate to describe the Rayleigh-Jeans tail of their SEDs. Indeed, most of the objects in Figure 1 group themselves around a value of $\alpha = 0 - 2$ on the power-law line. Lower redshift (older) stellar populations will appear redder in these passbands, both from their intrinsic SED shapes and from the K -corrections, and thus have larger values of α . The two dotted lines represent approximate $2\text{-}\sigma$ photometric error boundaries and mark the limits of the general “field” object distribution (open squares). Below this field distribution on the plot lies a group of objects (filled squares) which have significant excess emission at 4100Å, likely Lyman- α emission at $z \simeq 2.4$.

There exists the possibility that a fraction of these candidates could be $z \simeq 0.097$ objects whose [OII] emission at 3727Å has entered the F410M filter. However the differential volume element at $z \simeq 2.4$ is ~ 100 times larger than at $z \simeq 0.097$, and any other emission lines between Lyman- α and [OII] strong enough to be detected, such as C IV or Mg II, would only come from objects that have much lower surface densities (*e.g.*, QSOs and/or powerful radio galaxies). Since no other strong emission lines exist between Lyman- α and [OII] for star-forming objects (Kinney *et al.* 1996), we therefore expect that at most a few of the candidates may turn out to be O II emission line galaxies (or others) at lower redshift. Approximate Lyman- α restframe equivalent widths were calculated from the F410M fluxes and are indicated along the righthand vertical axis of Figure 1. If the excess 4100Å emission is interpreted as Lyman- α emission, it can be seen that most candidates have Lyman- α equivalent widths more consistent with typical “case B” recombination (*i.e.*, $< 100\text{\AA}$) rather than with the existence of an AGN. The restframe ultraviolet reddening vector (Seaton 1979) expected at $z \simeq 2.4$ is indicated, and suggests that the few reddest candidates may have a visual absorption of $A_V \lesssim 2\text{--}3$ mag. These reddest candidates should be viewed with some caution, however, because of the slight dependence of the B_{F450W} magnitudes on $B_{F450W} - V_{F606W}$ color. This effect increases towards redder color (Holtzman *et al.* 1995), in the sense that these very red objects appear somewhat lower on the plot than they should, and therefore could be contaminating field objects.

The 145 objects from Cycle 6 (Fig. 1) are plotted in Figure 2 along with the 115 objects from P96b for comparison. Unfilled symbols below the $2\text{-}\sigma$ lower boundary are candidates that have been rejected by inspection (*i.e.*, they are very bright and have diffraction spikes in the *WFPC2* images, indicating they are likely galactic stars) and/or by spectroscopy. The

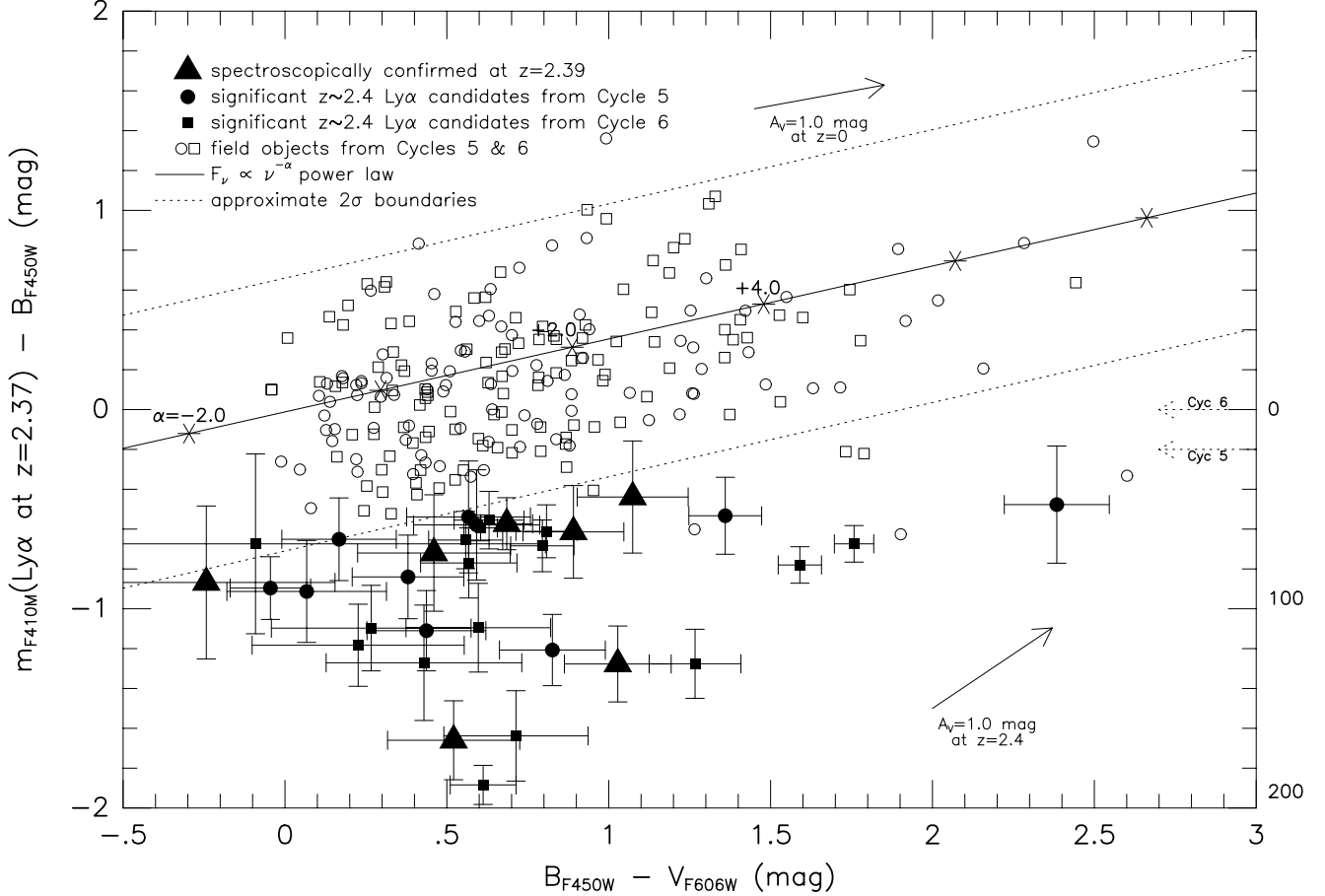


Fig. 2.— The same $(m_{F410M} - B_{F450W})$ versus $(B_{F450W} - V_{F606W})$ color-color diagram as in Figure 1, this time containing all objects from Cycles 5 and 6. The squares (open and filled) are from the three Cycle 6 parallel fields, and the circles (open and filled) are from the Cycle 5 observations of the 53W002 field. Filled symbols are $z \simeq 2.4$ candidates, and the filled triangles are objects from Cycle 5 that have been spectroscopically confirmed to be at $z \simeq 2.4$. Note the consistency of the photometry in that both sets of field objects fall on top of each other. The median $(B_{F450W} - V_{F606W})$ colors of the candidates are 0.57 mag and 0.60 mag for the Cycle 5 and Cycle 6 data respectively. The two dotted arrows on the right side of the figure represent the approximate completeness limits imposed by the F410M observations for Cycles 5 and 6.

Table 2: Cycles 5 and 6 $z \simeq 2.4$ Candidates

No.	α (J2000)	δ (J2000)	B_{F450W}	V_{F606W}	I_{F814W}	EW(Ly α) ^a	r_e ^b	z
1	17:14:10.53	50:15:09.80	26.0	24.5	24.2	35.0	0.16	-
5	17:14:13.54	50:15:34.73	24.4	24.3	24.0	66.5	0.15	-
6	17:14:14.74	50:15:28.91	23.4	22.6	21.9	38.0	0.72	2.390
8	17:14:06.83	50:16:02.60	26.2	25.6	25.5	49.9	0.10	2.386
11	17:14:12.63	50:15:36.75	25.6	24.5	24.0	28.4	0.30	-
12	17:14:11.66	50:15:49.36	25.2	24.2	23.7	41.2	0.24	2.388
13	17:14:10.98	50:15:54.26	26.3	23.9	22.0	31.0	0.12	-
18	17:14:11.89	50:16:00.51	23.6	23.0	22.3	179.6	-	2.393
19	17:14:11.27	50:16:08.72	24.1	23.0	22.2	113.0	0.36	2.397
29	17:14:18.89	50:16:21.24	27.1	27.3	27.2	63.7	0.16	-
34	17:14:13.44	50:16:57.08	25.1	24.8	24.3	44.1	0.20	-
37	17:14:20.24	50:15:50.16	25.5	25.4	24.4	68.2	0.18	-
40	17:14:20.76	50:15:41.83	25.5	25.0	24.0	90.6	-	-
60	17:14:08.16	50:15:52.76	25.8	25.2	24.9	38.4	0.28	-
61	17:14:08.53	50:15:52.22	26.3	25.7	25.4	35.5	0.17	-
94	17:14:21.98	50:15:36.75	24.9	24.0	23.3	103.2	-	-
113	17:14:16.84	50:16:00.16	25.7	25.2	24.4	60.9	0.08	-
213	21:07:32.11	-05:22:02.59	22.9	-	21.4	13.8	0.07	-
222	21:07:30.25	-05:21:29.86	24.1	-	19.8	19.3	0.12	-
230	21:07:30.92	-05:22:38.95	26.2	-	25.0	65.4	0.37	-
301	16:36:29.45	82:34:45.65	27.2	-	27.1	477.0	0.09	-
309	16:36:44.44	82:35:38.43	25.1	-	23.7	39.2	0.33	-
314	16:36:42.33	82:34:47.00	26.4	-	24.6	163.9	0.31	-
316	16:36:49.01	82:33:16.36	25.2	-	23.7	229.8	0.41	-
321	16:37:08.00	82:33:56.15	24.3	-	20.4	55.9	0.28	-
326	16:37:11.38	82:34:03.39	25.1	-	23.5	39.2	0.32	-
337	16:36:13.27	82:33:31.59	25.2	-	23.2	39.2	0.52	-
338	16:36:12.78	82:33:56.77	25.3	-	23.8	55.9	0.31	-
339	16:36:18.22	82:33:53.24	25.7	-	22.6	113.8	0.14	-
342	16:36:34.47	82:33:20.26	24.6	-	22.6	55.9	0.30	-
343	16:36:04.83	82:34:06.17	>27.8	-	>27.5	-	-	-
416	10:24:38.27	47:03:23.18	25.8	-	25.2	87.4	0.32	-
422	10:24:39.87	47:03:24.74	26.6	-	26.7	47.1	0.23	-
450	10:24:44.37	47:05:33.81	25.8	-	25.1	87.4	0.14	-
459	10:24:39.74	47:05:56.63	25.9	-	24.4	87.4	0.25	-

^aEstimated from the F410M and F450W fluxes

^bMean of effective radius measured in each available broadband (B_{F450W} , V_{F606W} , and I_{F814W} for the 53W002 field; B_{F450W} and I_{F814W} for the parallel fields)

median $B_{F450W}-V_{F606W}$ color (0.60 mag) of the Cycle 6 candidates (filled squares) is fairly consistent with that of the Cycle 5 objects (0.57 mag, filled circles), seven of which have thus far been spectroscopically confirmed (triangles). The histogram of Figure 3 shows that, for the most part, the photometry of the field objects from all four sets of data agree with each other. The calculated mean of the residuals of the four fields is only (-0.07 ± 0.01) , giving us confidence in the photometry despite the different observing times and pointings, and the somewhat different exposure times and filter sets. The photometry for all candidates, along with coordinates, Lyman- α equivalent widths, half-light radii, and redshifts (when known) are given in Table 2.

3.2. Sizes

Effective radii were determined for all the candidates following the method used in P96b, in which concentric elliptical isophotes, allowed to vary in ellipticity and position angle, were fit to the two-dimensional object images (see also Windhorst *et al.* 1994a,c; Odewahn *et al.* 1996; Mutz *et al.* 1997; Schmidtke *et al.* 1997 for details). The resulting size distribution is illustrated in Figure 4a, which also contains the Cycle 5 F410M candidates (shaded) for comparison. The new candidates are similarly compact, with typical $r_e \lesssim 0''.2$, which is smaller than the typical *WFPC2* galaxy scale lengths at these faint magnitudes ($\lesssim 0''.3-0''.4$ at $B \lesssim 27$, Odewahn *et al.* 1996). Several of the Cycle 6 objects fall into the $r_e = 0''.3-0''.35$ bin, possibly due to spurious detections that are not $z \simeq 2.4$ objects, or (more likely) due to the inherently lower signal-to-noise of these images and the corresponding difficulty in determining the proper sky level. Windhorst, Van Heerde, & Katgert (1984) showed that image noise can lead to an overestimate of measured sizes by $\sim 0.2-0.3$ dex. It is also possible that some fraction of the $z \simeq 2.4$ candidates are as large as $r_e = 0''.3$.

3.3. Luminosities

The luminosity distribution of all the candidates from Cycles 5 (shaded) and 6 is shown in Figure 4b. Absolute magnitudes were determined from the observed F606W magnitudes using the mean redshift ($z=2.39$) of the confirmed objects and K -corrections from a galaxy SED of Bruzual & Charlot (1993) as in Windhorst *et al.* (1991). K -band magnitudes for several of the candidates from recent IRTF observations of the 53W002 field (Keel *et al.* 1998) show a typical starburst spectrum, fairly flat in F_λ , so we can do the K -corrections without any additional assumptions. It can be seen in Figure 4b that all data sets contain mostly sub- L^* objects, assuming they are all at $z \simeq 2.4$. In particular, a majority of the

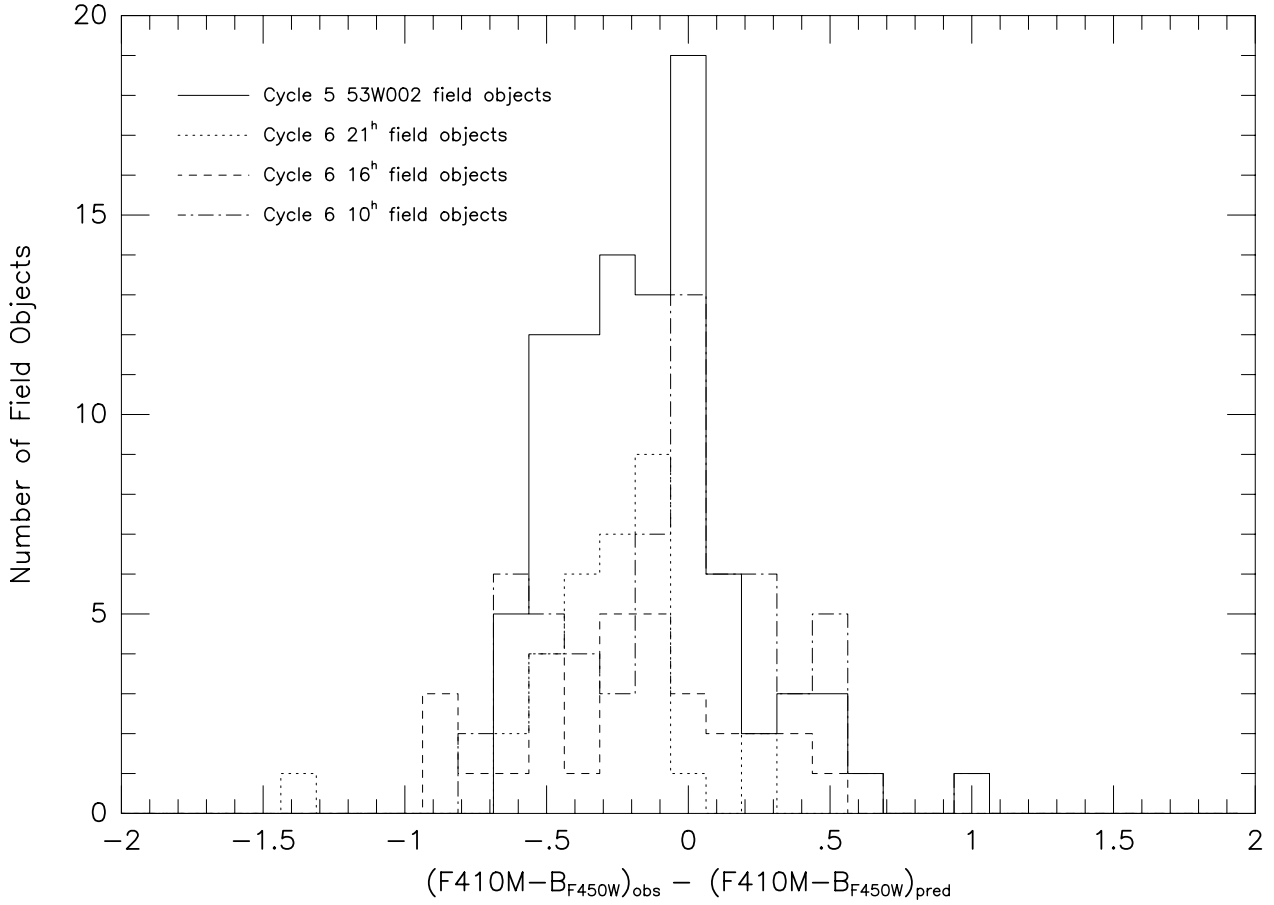


Fig. 3.— Histogram of the deviations of the field objects $(F410M - F450W)_{obs}$ from the power-law line $(F410M - F450W)_{pred}$ for the four separate sets of data. The $z \simeq 2.4$ candidates were not included in the calculations, so that an indication of the overall consistency of the photometry could be represented. It can be seen that they agree extremely well with each other, despite the various exposure times and pointings.

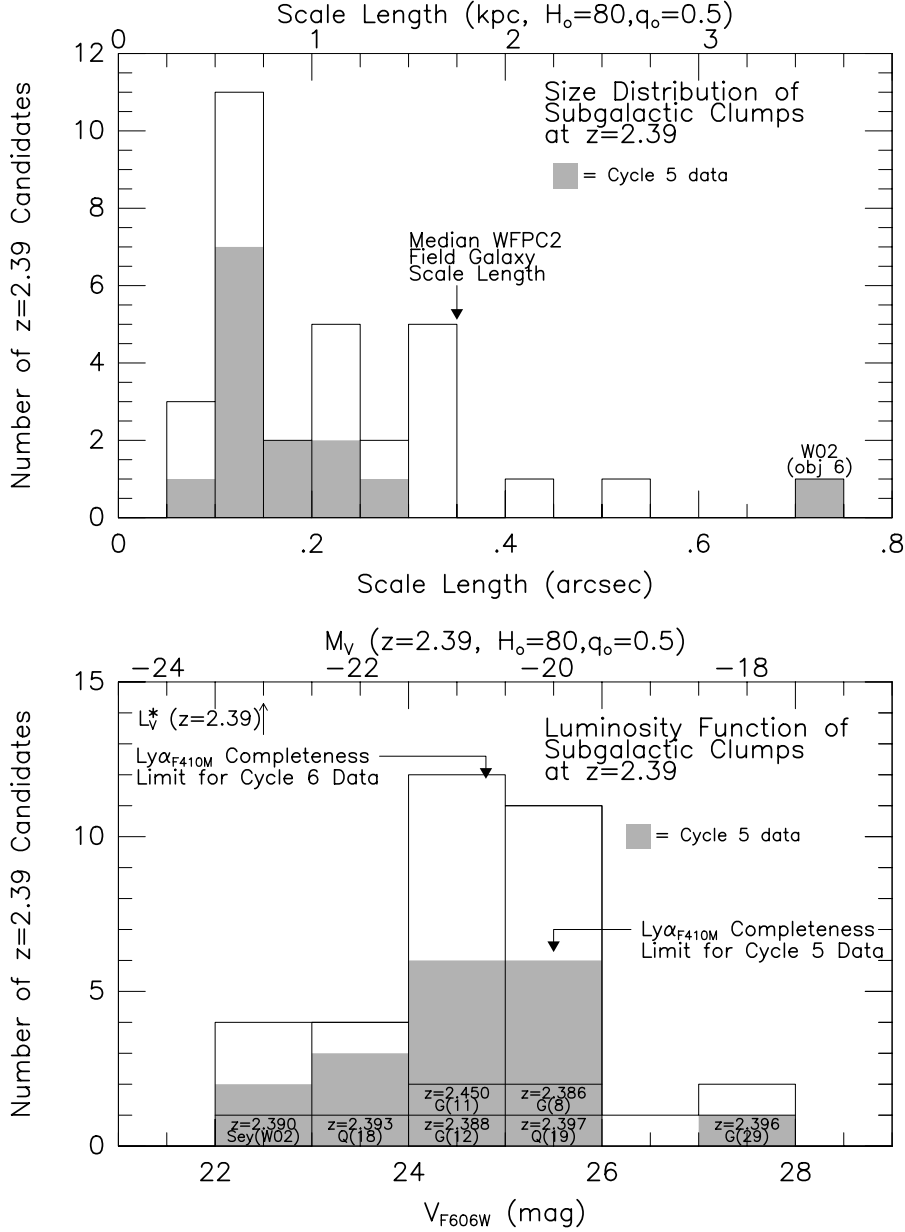


Fig. 4.— (a) Size distribution for the $z \simeq 2.4$ candidates. Except for a few extra objects in the $0^{\circ}30 - 0^{\circ}35$ bin, the Cycle 6 data generally agree with that of the 53W002 field, in that most candidates are very compact ($r_e < 0''.2$), (b) Luminosity distribution for the $z \simeq 2.4$ candidates in V_{F606W} . An absolute magnitude scale is given along the top axis, and the (evolving) value for L^* is indicated by the arrow. In both panels, the Cycle 5 data are represented by the shaded regions, and the Cycle 6 data by the white area. The agreement among the Cycles 5 and 6 data sets is very good. (Note that $q_0=0.5$ and $H_0=80$ are used here for direct comparison to the P96b data.)

candidates have $M_V \simeq -20.5$ to -21.5 mag, despite the different completeness limits imposed by the shallower F410M exposures (as indicated by the dotted arrows at the right of Figure 2). The value for L^* ($M_V \simeq -23$ mag) was calculated by assuming that there would have been ~ 2 mag of stellar evolution since $z \simeq 2.4$ for a typical starburst ~ 0.3 – 0.5 Gyr earlier, as the unreddened blue colors of the candidates suggest (Bruzual & Charlot 1993). The adopted ~ 2 mag of luminosity evolution has an uncertainty of $\simeq 0.50$ – 0.75 mag and comes from the models used in Windhorst *et al.* (1991) for 53W002. As described in P96b, a point source was subtracted from three of the Cycle 5 candidates that contain an AGN based on their spectra before being added to the histogram. No attempt was made to fit point source contributions to any candidates without spectroscopically known AGN.

4. Discussion

4.1. Galaxy Formation at High Redshift

In models of hierarchical galaxy formation, the luminous galaxies we see today were built up through the repeated merging of smaller protogalactic pieces. A significant number of such sub-galactic clumps may have been found at $z \simeq 2.4$ by P96b in a field surrounding the radio galaxy 53W002 at $z=2.390$. There has been a recent series of reports of very high redshift, “normal” star-forming galaxies with possibly greater scale lengths and higher luminosities (*e.g.*, Hu & McMahon 1996; Madau *et al.* 1996; Steidel *et al.* 1996a and 1996b; Yee *et al.* 1996; Francis, Woodgate, & Danks 1997; Lowenthal *et al.* 1997; Trager *et al.* 1997). The Steidel *et al.* (1996a,b) Madau *et al.* (1996), and Lowenthal *et al.* (1997) galaxies were found through their *U*-band or *B*-band “dropout,” caused by the Lyman break in their spectra, and not via emissions lines, which may explain why they may be more luminous than the $z \simeq 2.4$ clumps of P96b (*i.e.*, a significant continuum detection was necessary to find them). In addition, only about 40–50% of these “dropout” galaxies are Lyman- α emitters, with the rest having either no Lyman- α emission or significant Lyman- α in absorption. The relatively stronger Lyman- α emitters like the sub-galactic clumps of P96b and this paper, and those reported by Hu & McMahon (1996) and Francis, Woodgate, & Danks (1997) were found likely because they have had fewer generations of O stars, and so fewer supernovae to produce significant dust to destroy the Lyman- α light.

These findings suggest that galaxies formed over a large range of redshift rather than at one special time, and possibly according to several different formation scenarios. If a large percentage of galaxies did in fact form hierarchically, we would expect to find their building blocks at high redshifts ($z \gtrsim 2$), consistent with the large number of star-forming objects currently being found at such high redshifts. Many studies seem to point toward a merger

rate that was higher in the past, following $\propto(1+z)^m$ with $m \simeq 2 - 4$ (Burkey *et al.* 1994; Carlberg, Pritchet, & Infante 1994; Yee & Ellingson 1995; Patton *et al.* 1997) and suggests that there should have been a higher space density of sub-galactic clumps at earlier epochs in order to produce the observed local luminosity function. Taken together with the fact that most luminous early-type galaxies appear to have been “in place” by $z \sim 1$ (Mutz *et al.* 1994; Driver *et al.* 1995a; Lilly *et al.* 1995; Odewahn *et al.* 1996; Heyl *et al.* 1997; Driver *et al.* 1998), these two points imply that a large fraction of today’s luminous ellipticals and early- to mid-type spirals formed at $z \gtrsim 1$, possibly from the merging of such sub-galactic sized objects. Indeed, it has been shown that disks can be regenerated (or generated) after such mergers, as gas remains bound to the system and falls back in (Hibbard & Mihos 1995; Tissera, Lambas, & Abadi 1997).

As shown in P96b, *HST* provides the resolution and sensitivity necessary for a search for such populations of faint compact objects. The fortunate existence of a medium-band *WFPC2* filter centered at 4100\AA (Lyman- α at $z \simeq 2.4$) allowed the discovery of the group of 17 candidate $z \simeq 2.4$ objects within $\sim 1\text{ Mpc}^2$ reported by P96b. A similar finding, using infrared filters to trace redshifted $\text{H}\alpha$, has been reported by Malkan, Teplitz, & McLean (1996) at $z \simeq 2.5$. The Cycle 6 images presented in this paper used the same medium-band *WFPC2* filter (F410M) to extend these results. Given that the Cycle 6 observations are $\sim 50\text{--}60\%$ as deep as the original 53W002 observations and the luminosity function is quite steep at this redshift, we would expect to find $< 8 - 10$ $z \simeq 2.4$ candidates in any random part of the sky if the candidates seen around 53W002 are indeed part of an isotropic widespread population. Here we assume that sensitivity roughly scales as the square root of the exposure time and that the 53W002 field is a representative high-redshift field. If, for some reason, possibly because of the existence of the weak radio source and/or because of the existence of several AGN surrounding 53W002 (Windhorst, Keel, & Pascarelle 1998), this field is not representative at $z \simeq 2.4$, then we should find very few (if any) significant $z \simeq 2.4$ candidates in any of the random field searches. However, we found three candidates in the 21^h field, 11 in the 16^h field, and four in the 10^h field (see Fig. 1).

4.2. Structure at $z \simeq 2.4$

Currently, there are seven spectroscopically confirmed out of the 17 total $z \simeq 2.4$ candidates in the 53W002 field with three negative confirmations (P96b; Armus *et al.* 1998). This implies a $\sim 70\%$ success rate for the medium-band method of finding Lyman- α emitting candidates at high redshift. To fairly compare the 53W002 field to the three Cycle 6 parallel fields, we must take into account the relative depths of the observations and the probable

steepness of the $z \simeq 2.4$ luminosity function. We consider all four fields only down to the F410M completeness limit of the *shallowest* parallel observation (the 21^h field at $m_{\text{F410M}}=25$ mag). The 53W002 field has ten candidates brighter than this magnitude limit, and assuming a $\sim 70\%$ success rate, this yields seven $z \simeq 2.4$ objects. The Cycle 6 data, for which we have not yet attempted any spectroscopy, will yield one object (out of the two candidates above the completeness limit) from the 21^h field, eight objects (out of the 11 candidates above the completeness limit) from the 16^h field, and two objects (out of the three candidates above the completeness limit) from the 10^h field. Clearly, the 16^h field is consistent with the 53W002 field, while the other two fields have a lower density. The most striking aspect of these data is the significant difference in the numbers of candidates from these four fields after correcting them to the depth of the 21^h field. For any two such fields, the significance of the different number densities can be represented by:

$$\frac{|N_1 - N_2|}{\sqrt{N_1 + N_2}}$$

This calculation, in which N_1 and N_2 are the numbers of candidates in each field, indicates that a 2σ difference exists between the 21^h (or 10^h) field and 53W002 (or 16^h) field. There are two possible reasons for this discrepancy. First, it may be an indication that the 53W002 and 16^h fields are *not* representative of high-redshift fields. This would mean that they may be a $\sim 2\sigma$ statistical fluctuation with respect to other fields, based on the numbers estimated above. Second, as noted in P96b, the confirmed 53W002 candidates show a remarkably small group velocity dispersion ($\simeq 286$ km/s), despite the much larger width of the F410M filter. We could have seen Lyman- α emission from objects in the entire redshift range $z \simeq 2.28 - 2.45$, although some dropoff in transmission would occur for $z \lesssim 2.30$ and $z \gtrsim 2.42$. This implies that the sub-galactic clumps may have existed to some extent in groups or clusters at high redshift, or else we should have seen a larger number of objects at other redshifts ($z \neq 2.391 \pm 0.004$) inside the F410M filter. Currently, we have found only one object (out of seven) which has a highly discrepant redshift ($z=2.451$), surprisingly far out into the red wing of the filter. Some level of clustering, therefore, can explain the statistically marginal variation in density of the candidates from field to field. Indeed, such a structure may have also been discovered at $z \simeq 3.0$ by Steidel *et al.* (1998), lending further evidence that large-scale structure may have existed at high redshifts.

The space density of the $z \simeq 2.4$ candidates from P96b is $\sim 0.038 \text{ Mpc}^{-3}$, assuming that Lyman- α lies somewhere within the F410M filter and a $\sim 70\%$ success rate (= 7 objects out of 10, if we consider candidates only down to the limiting F410M magnitude of the shallowest parallel observation). Under the same assumptions, we find space densities of $\sim 0.0054 \text{ Mpc}^{-3}$, $\sim 0.043 \text{ Mpc}^{-3}$, and $\sim 0.011 \text{ Mpc}^{-3}$ for the 21^h, 16^h, and 10^h fields respectively. One can see that the 53W002 and 16^h fields could be a factor of 3–4 times more dense than the

other two Cycle 6 fields. Unlike the 53W002 field, the 16^h field was not targeted around an *a priori* known density fluctuation such as that which might be expected in the field surrounding the weak radio galaxy 53W002. It is interesting to note that the 10^h field, which has a comparatively lower space density of candidates, was imaged in parallel to an FOC observation of the lensed object IRAS 10214+4721 at $z=2.30$, so that any associated large-scale structure would be just within our sensitivity range.

The variation in number density among the Cycle 5 and 6 fields, if significant, is indeed suggestive of the existence of some kind of structure (*e.g.*, groups, clusters, or “sheets” at $z \simeq 2.4$). We appear to have hit such a structure in the 53W002 and 16^h fields, but are perhaps looking “in between” any such major structures in the 21^h and 10^h fields. The small velocity dispersion of the confirmed 53W002 field objects implies that we may be viewing such a sheet more “face-on” than “edge-on,” since the velocity dispersion would likely be much higher if a, *e.g.*, $\gtrsim 128$ Mpc structure (*cf.*, Broadhurst *et al.* 1990; Landy *et al.* 1996; Le Fèvre *et al.* 1994) was viewed edge-on. A picture is beginning to develop here which is quite consistent with that of RHS97, in which luminous galaxies at $z=0$ are broken up into several individual clumps at higher redshifts and are embedded in sheet- or ribbon-like structures, often lying along filaments on these sheets. These sheets appear to be group or sub-cluster size, and may represent the preferred environment for the formation of high-redshift objects. Even the somewhat higher luminosity objects of Steidel *et al.* (1996a,b), Madau *et al.* (1996), and Lowenthal *et al.* (1997) seem to show hints of this structure, with several pairs and triplets having very similar redshifts (three of five redshifts of star-forming Lyman-limit “drop-out” galaxies in the HDF from Steidel *et al.* (1996a) are at $z \sim 2.8$). Also, there is the significant peak in $N(z)$ at $z \simeq 3.0$ over an $11' \times 8'$ area on the sky recently reported by Steidel *et al.* (1998).

4.3. The Luminosity Function of $z \simeq 2.4$ Candidates

We attempt to construct a LF for the $z \simeq 2.4$ candidates from all four *WFPC2* fields based on their F450W luminosities. The *WFPC2* synthetic magnitudes were converted to AB magnitudes and number densities were calculated using the comoving volume defined by the redshift range of the F410M passband and the angular size of the *WFPC2* field at $z \simeq 2.4$. To properly represent the fainter luminosity bins, in which the shallower parallel fields become incomplete, we omit candidates from fields that are not fully complete in any given luminosity bin. The corresponding volume used in the number density calculation is decreased accordingly, and the result is a fair indication of the luminosity function of Lyman- α emitting candidates at $z \simeq 2.4$, if the 53W002 field is representative at this redshift. We

plot these data in Figure 5 as the filled triangles.

For comparison, we include in Figure 5 a Schechter LF fit (solid curve) to the $z=2-3$ HDF field galaxy data, represented by the filled squares, from Sawicki, Lin, & Yee (1997, hereafter SLY97). SLY97 find from photometric redshifts a LF for galaxies in the HDF that changes with redshift, showing both a brightening and steepening of the HDF LF with increasing redshift up to $z \sim 3$. Their data are in agreement with the LF of deep galaxy redshift surveys at $z \lesssim 1$, *e.g.*, the CFRS (Lilly *et al.* 1995, 1996; LeFevre *et al.* 1996). SLY97 point out that the flattening of the faint-end slope of the HDF luminosity function is an expected result of hierarchical models of galaxy formation, in which merging plays an important role in removing the sub-galactic clumps at lower redshifts.

As can be seen in Figure 5, our $z \simeq 2.4$ LF is quite consistent with that of the HDF of SLY97 for $2 < z < 3$ to about $M_{F450W_{AB}} \simeq -19.5$, below which the completeness limit of $M_{F450W_{AB}} \simeq -19$ mag imposed by our much shallower F410M observations takes over. Our points are slightly lower than the SLY97 data, but the results of Steidel *et al.* (1996a,b), Lowenthal *et al.* (1997), and Trager *et al.* (1997) show that as much as 50% of their $z=2-3$ objects lack significant Lyman- α emission. Correcting our data for this would move our points up by a small amount (~ 0.3 dex). We show the corrected data points as the empty triangles. The consistency, to within the errors, of our data with that of SLY97 after correcting for this factor of two supports the idea that the $z \simeq 2.4$ clumps are a significant contribution to the faint-end $z=2-3$ galaxy counts ($\sim 50\%$).

It should be mentioned in this context that the scientific return from a minimal investment of exposure time in the HDF and in the upcoming HDF South through the F410M and F467M filters would be considerable, since all the broadband *UBVI* data are (or will be) in hand. This would be an excellent direct determination of the space density of high-redshift, Lyman- α emitting sub-galactic clumps.

5. Conclusions

We have obtained Cycle 6 *HST* images of three random fields with the *WFPC2* F410M filter to test the idea that the sub-galactic clumps reported by P96 are not unique to the 53W002 field (due to the presence of the radio galaxy) but are a widespread population that exist all over the sky. We also attempt to use the data to constrain whether or not these objects tend to be in groups or clusters at high redshift. We have found a total of 18 candidate Lyman- α emitting objects in the three parallel *HST* fields, of which ~ 13 are expected to be spectroscopically confirmed if we assume the current success rate for the

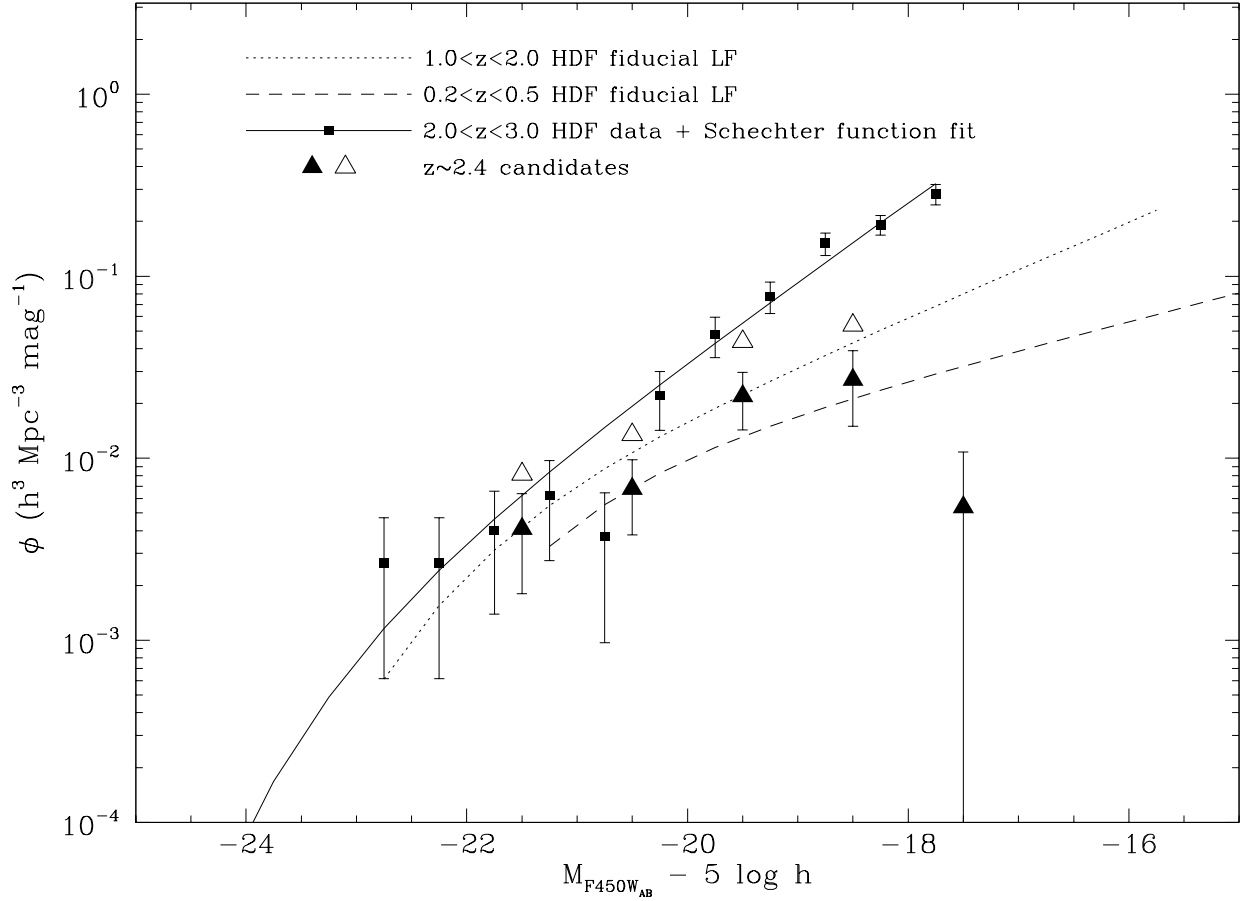


Fig. 5.— Luminosity function of the Cycle 6 data (filled triangles) plotted with the SLY97 $z=2-3$ HDF data. The data were converted to AB magnitudes according to SLY97, and number densities were calculated using the comoving volume defined by the redshift range of the F410M passband and the angular size of the *WFPC2* field at $z \simeq 2.4$. The solid line is a Schechter luminosity function fit to the HDF data, represented by the filled squares. Dashed and dotted lines are fiducial LFs from other redshift bins of the SLY97 data. Our points are slightly lower than the SLY97 data, but the results of Steidel *et al.* (1996a,b), Lowenthal *et al.* (1997), and Trager *et al.* (1997) show that as much as 50% of their $z=2-3$ objects lack significant Lyman- α emission. We corrected our data for this by moving our points up by a small amount (~ 0.3 dex), as indicated by the empty triangles.

53W002 field ($\sim 70\%$). Most of these candidates appear to be as faint and compact as the Cycle 5 objects, implying that the 53W002 field is not unique, and that these faint subgalactic clumps were quite common at early epochs. Perhaps it is not that surprising to find $z \simeq 2.4$ objects all over the sky in light of the large number of $z \simeq 3$ objects of Steidel *et al.* (1998), as well as photometric redshift samples that find peaks in the redshift distribution close to this value (*e.g.*, Gwyn & Hartwick 1996 in the HDF) and point to a peak for star formation in disk galaxies at $z \simeq 1 - 2$ (Pei & Fall 1995; Madau *et al.* 1996; Connolly *et al.* 1997). The relatively large difference in the object counts of the three fields also hints that these objects may preferentially exist in groups, clusters, or “sheets,” not unlike the theoretical picture presented by RHS97.

Because of the existence of only two *WFPC2* filters on *HST* suitable for finding compact emission-line objects (the F410M and F467M filters), we were limited in the number of redshifts we could search ($z \simeq 2.4$ and $z \simeq 2.8$). The narrow-band filters available to *WFPC2* are not wide enough to sample more than a fraction of a single redshift “sheet,” if galaxies trace such structures at high redshifts as they appear to at low redshifts (Landy *et al.* 1995; Cohen *et al.* 1996). From this perspective, the narrow *HST* filters are rather unsuitable for the purpose of locating larger numbers of high-redshift Lyman- α emitting objects. It should also be noted that such observations will not be possible with the Advanced Camera because it does not have the appropriate medium-band filter set, and the field-of-view of its linear ramp filters is too small.

The Cycles 5 and 6 data offered us a unique opportunity to examine the $z \simeq 2.4$ epoch, but similar observations with the F467M filter on *HST* and with (hopefully) a more extensive filter set on the Next Generation Space Telescope will surely need to be carried out. Indeed more random observations in F410M itself are still necessary to confirm these initial findings and improve upon our statistics.

SMP acknowledges support from NASA grant NAGW-4422, NSF grant AST-9624216, and a NASA Space Grant Fellowship. RAW and SMP acknowledge support from *HST* grants GO.5985.01.94A and GO.6610.01.95A, and WCK acknowledges support from *HST* grants GO.6610.02.95A and GO.5985.02.94A. We would also like to thank Doug van Orsow for help in scheduling the Cycle 6 parallel observations, Anne Cowley and David Burstein for a careful reading of the manuscript, and Marcin Sawicki for graciously allowing us to use the SLY97 HDF plot.

REFERENCES

- Armus, L., Pascarelle, S. M., Scoville, N. Z., & Windhorst, R. A. 1998, ApJ (in preparation)
- Broadhurst, T. J., Ellis, R. S., Koo, D. C., & Szalay, A. S. 1990, Nature, 343, 726
- Bruzual, A. G., & Charlot, S. 1993, ApJ, 405, 538
- Burkey, J. M., Keel, W. C., Windhorst, R. A., & Franklin, B. E. 1994, ApJ, 429, L13
- Carlberg, R. G., Pritchet, C. J., & Infante, L. 1994, ApJ, 435, 540
- Connolly, A. J., Szalay, A. S., Dickinson, M., SubbaRao, M. U., & Brunner, R. J. 1997, ApJ, 486, L11
- Cohen, J. G., Cowie, L. L., Hogg, D. W., Songaila, A., Blandford, R., Hu, E. M., & Shopbell, P. 1996, ApJ, 471, L5
- Diaferio, A., & Geller, M. J. 1997, ApJ, 481, 633
- Driver, S. P., Windhorst, R. A., Ostrander, E. J., Keel, W. C., Griffiths, R. E., & Ratnatunga, K. U. 1995a, ApJ, 449, 23
- Driver, S. P., Fernández-Soto, A., Couch, W. J., Odewahn, S. C., Windhorst, R. A., Phillips, S., Lanzetta, K. M., & Yahil, A. 1998, ApJ, 496, L93
- Ettori, S., Guzzo, L., & Tarenghi, M. 1997, MNRAS, 285, 218
- Francis, P. J., Woodgate, B. E., & Danks, A. C. 1997, ApJ, 482, L25
- Gwyn, S. D. J. & Hartwick, F. D. A. 1996, ApJ, 468, 77
- Heyl, J., Colless, M., Ellis, R. S., & Broadhurst, T. 1997, MNRAS, 285, 613
- Hibbard, J. E., & Mihos, J. C. 1995, AJ, 110, 140
- Holtzman, J. A., Burrows, C. J., Casertano, S., Hester, J. J., Trauger, J. T., Watson, A. M., & Worthey, G. 1995, PASP, 107, 1065
- Hu, E. M., & McMahon, R. G. 1996, Nature, 382, 281
- Keel, W. C., Pascarelle, S. M., & Windhorst, R. A. 1998, ApJ (in preparation)
- Kinney, A. L., Calzetti, D. A., Bohlin, R. C., McQuade, K., Storchi-Bergmann, T., & Schmitt, H. R. 1996, ApJ, 467, 38
- Landy, D. L., Shectman, S. A., Lin, H., Kirshner, R. P., Oemler, A. A., & Tucker, D. 1996, ApJ, 456, L1
- Le Fèvre, O., Crampton, D., Hammer, F., Lilly, S. J., & Tresse, L. 1994, ApJ, 423, L89.
- Le Fèvre, O., Hudon, D., Lilly, S. J., Crampton, D., Hammer, F., & Tresse, L. 1996, ApJ, 461, 534

- Lilly, S. J., Tresse, L., Hammer, F., Crampton, D., & Le Fèvre, O. 1995, *ApJ*, 455, 108
- Lilly, S. J., & Le Fèvre, O., Hammer, F., & Crampton, D. 1996, *ApJ*, 460, L1
- Lowenthal, J. D. *et al.* 1997, *ApJ*, 481, 673
- Madau, P., Ferguson, H. C., Dickinson, M., Giavalisco, M., Steidel, C. C., & Fruchter, A. 1996, *MNRAS*, 283, 1388
- Malkan, M. A., Teplitz, H., & McLean, I. S. 1996, *ApJ*, 468, L9
- Mutz, S. B. *et al.* 1994, *ApJ*, 464, L55
- Mutz, S. B., Windhorst, R. A., Wittman, D., Close, L. M., & McCarthy, D. W. 1997, *AJ*, 113, 1537
- Odewahn, S. C., Windhorst, R. A., Driver, S. P., & Keel, W. C. 1996, *ApJ*, 472, L13
- Pascarelle, S. M., Windhorst, R. A., Driver, S. P., Ostrander, E. J., & Keel, W. C. 1996a, *ApJ*, 456, L21
- Pascarelle, S. M., Windhorst, R. A., Keel, W. C. & Odewahn, S. C. 1996b, *Nature*, 383, 45
- Patton, D. R., Pritchet, C. J., Yee, H. K. C., Ellingson, E., & Carlberg, R. G. 1997, *ApJ*, 475, 29
- Pei, Y. C., & Fall, S. M. 1995, *ApJ*, 454, 69
- Press, W. H., & Schechter, P. 1974, *ApJ*, 187, 425
- Rauch, M., Haehnelt, M. G., & Steinmetz, M. 1997, *ApJ*, 481, 601
- Sawicki, M. J., Lin, H., & Yee, H. K. C. 1997, *AJ*, 113, 1
- Seaton, M. J. 1979, *MNRAS*, 187, 73P
- Schmidtke, P. C., Windhorst, R. A., Pascarelle, S. M., & Franklin, B. E. 1997, *AJ*, 113, 569
- Steidel, C. C., Giavalisco, M., Pettini, M., Dickinson, M., & Adelberger, K. L. 1996a, *ApJ*, 462, L17
- Steidel, C. C., Giavalisco, M., Dickinson, M., & Adelberger, K. L. 1996b, *AJ*, 112, 352
- Steidel, C. C., Adelberger, K. L., Dickinson, M., Giavalisco, M., Pettini, M., & Kellogg, M. 1998, *ApJ*, 492, 428
- Thompson, D., Mannucci, F., & Beckwith, S. V. W. 1996, *AJ*, 112, 1794
- Thompson, D., Djorgovski, S., & Trauger, J. 1995, 110, 963
- Tissera, P. B., Lambdas, D. G., & Abadi, M. G. 1997, *MNRAS*, 286, 384
- Trager, S. C., Faber, S. M., Dressler, A., & Oemler, A. O. 1997, *ApJ*, 485, 92
- White, S. D. M., & Rees, M. J. 1978, *MNRAS*, 183, 341

- Windhorst, R. A., Van Heerde, G. M., & Katgert, P. 1984, *A&A*, 58, 1
- Windhorst, R. A. *et al.* 1991, *ApJ*, 380, 362
- Windhorst, R. A. *et al.* 1994a, *AJ*, 107, 930
- Windhorst, R. A., Franklin, B. E., & Neuschaefer, L. W. 1994b, *PASP*, 106, 798
- Windhorst, R. A., Gordon, J. M., Pascarelle, S. M., Schmidtke, P. C., Keel, W. C., Burkey, J. M., & Dunlop, J. S. 1994c, *ApJ*, 435, 577
- Windhorst, R. A., Keel, W. C., & Pascarelle, S. M. 1998, *ApJ*, 494, L27
- Yee, H. K. C., & Ellingson, E. 1995, *ApJ*, 445, 37
- Yee, H. K. C., Ellingson, E., Bechtold, J., Carlberg, R. G., & Cuillandre, J.-C. 1996, *AJ*, 111, 1783